RSC Advances

PAPER

View Article Online
View Journal | View Issue

Cite this: *RSC Adv.*, 2024, **14**, 27122

Bioengineering of one dimensional hierarchical Cu_7S_4 hollow nanotubes for non-enzymatic glucose sensing applications†

Giday G. Welegergs, *[ab] Abera D. Ambaye,[c] Mbulelo Jokazi,[a] Nnamdi Nwahara[a] and Tebello Nyokong [a]

Herein, a novel and facile eco-friendly green chemistry approach has been devised at room temperature for synthesis of 1D hierarchical Cu_7S_4 hollow nanotubes on Cu substrate *via* volatile organosulfur compounds from *Allium sativum* L for non-enzymatic glucose detection. Field emission scanning electron microscopy (FESEM), transmission electron microscopy (TEM), X-ray diffraction (XRD), energy dispersive X-ray spectroscopy (EDX), and X-ray spectroscopy (XPS) were employed to characterize the surface morphology, structural phase, compositional, and chemical states of the obtained samples, respectively. The SEM results confirm the formation of 1D hierarchical Cu_7S_4 hollow nanotubes. The XRD patterns are indexed to orthogonal anilite Cu_7S_4 crystal planes and the EDX spectra clearly reveal the presence of Cu and S elements. XPS spectra confirms peaks of Cu 2p and S 1s core levels, which are typical characteristics of Cu(I) and S(II), respectively. The Brunauer–Emmett–Teller (BET) specific surface area for obtained Cu_7S_4 hollow nanotubes is 2.07 $m^2\ g^{-1}$ with a pore size distribution of 27.90 nm. Using Cu_7S_4 hollow nanotubes, the detection of non-enzymatic glucose was conducted over a dynamic range of concentrations from 0.5 to 100 μmol L^{-1} and reveals a high sensitivity of 1058.33 μA $mM^{-1}cm^{-2}$ and a limit of detection (LOD) of 0.127 μmol L^{-1}. The obtained results indicated that Cu_7S_4 hollow nanotubes are promising candidates for non-enzymatic glucose detection.

Received 17th July 2024
Accepted 21st August 2024

DOI: 10.1039/d4ra05199h

rsc.li/rsc-advances

1 Introduction

Diabetes is a leading cause of death, resulting primarily from high blood glucose levels. Projections indicate that by 2045, over 783 million individuals could be affected, exceeding 10% of the global population. Therefore, rapid, responsive, and specific detection of glucose is of significant concern across various scientific and technological domains, encompassing healthcare, food, and environmental surveillance.[1–7] Importantly chemical sensors are vital technologies and devices that record the physical, chemical, and/or biological changes of a material and convert them into measurable signals for various applications.[8–10]

Most commercialized disposable glucose sensors are fabricated by use of highly optimized cocktails and these sensors are based on chronoamperometric detection of hydrogen peroxide. This has led to manufacturing of glucose test strips and commercialization of glucometer devices, that are currently available in the market. Electrochemical glucose sensors are mainly classified into glucose oxidase (GOx) enzyme-based and non-enzymatic glucose sensors. Electrochemical glucose sensors based on enzyme immobilization methods such as, sol–gel adsorption, direct adsorption, cross-linking, *etc.* have been widely studied and utilized in line with the cocktail methods.[10–12] All types of enzyme-modified sensor electrodes necessitate complicated enzyme fixation and thus inevitably suffer from insufficient stability issues because of the nature of the enzymes due to their sensitivity to changes in humidity, pH, temperature, toxic chemicals, and interference of some electro-oxidizable species. In order to solve these problems, non-enzymatic glucose biosensors have been proposed, which have the advantages of sensitivity, high stability, fast response, affordability, portability, scalability, and ease of preparation. Electrochemical non-enzymatic biosensors involve directly depositing a sensing material onto the electrode surface, enabling unrestricted ion/electron flow and enhancing conductivities.[1,10,13–23]

Recently, transition metal chalcogenides (TMCs) have received great attention and exploited for a wide range of applications such as environmental screening, catalysis, photovoltaics, biomedical diagnosis and therapy because of their lower cost, natural abundance, and environmentally

[a]*Institute for Nanotechnology Innovation, Rhodes University, Makhanda 6140, South Africa. E-mail: getgiday@gmail.com*

[b]*Debre Berhan University, Department of Chemistry, P. O. Box 445, Debre Berhan, Ethiopia*

[c]*Materials Science and Engineering, Bio, and Emerging Technology Institute, 5954, Addis Ababa, Ethiopia*

† Electronic supplementary information (ESI) available. See DOI: https://doi.org/10.1039/d4ra05199h

friendliness, higher electrical conductivity and richer redox valences.[17–19] Among the transition chalcogenides, copper sulfide (Cu_xS, x = 1–2) is one of the most important semiconductors with a lower band gap of 1.2–2.4 eV and has an inevitable place as a promising material due to its special properties and potential applications. Interestingly, copper sulfide exists in variable stable stoichiometric phases, which have been experimentally reported and range from the copper-rich phases of chalcocite (Cu_2S), digenite (Cu_9S_5), and roxbyite/anilite (Cu_7S_4) to the copper-deficient phases: covellite (CuS) and villamaninite (CuS_2). All copper sulfides are essentially of p-type semiconductor nature ascribed to the existence of Cu vacancies in the crystal lattices.[24–28] Copper sulfides have been explored as potential candidates for the development of non-enzymatic glucose sensors because of their interesting properties like electrical conductivity.[29–31] For example, S. Radhakrishnan *et al.*[32] successfully synthesized CuS microflower (MF) superstructure *via* facile solvothermal method for nonenzymatic glucose detection. This CuS MF modified electrode showed an excellent sensitivity (1007 μA mM^{-1} cm^{-2}) at 0.5 V with a good anti-interference ability and long-term stability. Miaomiao Cao *et al.*[33] also reported copper sulfides by varying the amount of Na_2S precursors and Cu_7S_4 hollow nanospheres demonstrated a wide linear concentration response towards non-enzymatic electrochemical glucose detection from 1–2.0 mM, with a LOD of 0.023 μM and high sensitivity of (3728.7 μA mM^{-1} cm^{-2}). However, the non-enzymatic glucose sensor based on hollow nanostructured Cu_xS has rarely been reported.

It is well known that electrochemical biosensing performance depends on the surface morphology of nanomaterials. Hollow nanostructured materials are the most effective in the field of diagnosis because of their unique structure and properties, which originate from their nanoscale hollow structures. Hollow nanomaterials consist of distinguishable interior cavities/voids and well-defined boundary functional shells that can effectively improve the electrocatalytic properties due to their lower density, high surface area, shell permeabilities, and sufficient space that allow for volume expansion and reduced transport paths for both mass and ion/electron transport.[33–35] To the best of our knowledge, Cu_7S_4 hollow nanotubes using green volatile organosulfur compounds from *Allium sativum* L for biosensing application has not been reported yet. *Allium sativum* L (garlic) is a common natural product and contains highly volatile bioactive organosulfur compounds responsible both for garlic pungent odour and many of its medicinal effects.[36] Herein, we explored biosulfurized 1D hierarchal Cu_7S_4 hollow nanotubes on a Cu substrate using volatile organosulfur compounds from *Allium sativum* L at room temperature as nano-catalysts for electrochemical non-enzymatic glucose sensing applications. The preparation, characterization, and chronoamperometric response of Cu_7S_4 electrode is reported in detail.

2 Experimental section

2.1 Materials and chemicals

The following reagents were employed: Copper substrates (Cu, 99.99%, Sigma-Aldrich Co., Ltd), sodium hydroxide (NaOH, 99%, Alfa-aesar Co., Ltd) D-glucose ($C_6H_{12}O_6$, ≥96.5%, Alfa-aesar Co., Ltd), D-fructose ($C_6H_{12}O_6$, 99%, Merck, Co., Ltd), lactose ($C_6H_{12}O_6$, 99%, Merck, Co., Ltd), galactose ($C_6H_{12}O_6$, 99%, Sigma-Aldrich, Co., Ltd), hydrogen peroxide (H_2O_2, 30–35%, Minema chemicals, Co., Ltd), uric acid ($C_5H_4N_4O_3$, 99%, Sigma-Aldrich, Co., Ltd), ascorbic acid ($C_6H_8O_6$, 99%, Sigma-Aldrich, Co., Ltd), oxalic acid (HO_2CCO_2H, 99%, Sigma-Aldrich, Co., Ltd), sodium sulfide hydrate (Na_2S, ≥60%, Sigma-Aldrich, Co., Ltd), sodium nitrate (NaNO3, 99%, BDH, Co., Ltd) and electrodes (Pt wire and Ag/AgCl). *Allium sativum* L was obtained from a local supermarket in South Africa. All reagents are analytical grade purity and were used without further purifications. Deionized water was used for all experimental works.

2.2 Synthesis of Cu_7S_4 hollow nanotubes

Intended for pure green chemistry synthesis of Cu_7S_4 on Cu-substrate, bioactive volatile organosulfur compounds from *Allium sativum* L (garlic) were used as a source of sulfur to biosulfurized the surface of the Cu substrate. Prior to the experiment, copper substrates (1.0 cm × 0.12 cm × 0.5 mm) were successively sonicated in acetone, ethanol, and deionized water for 15 min each and dried by blowing of N_2 gas. Typically, 60 g of *Allium sativum* cloves were peeled and chopped using an electrical blender being inserted it into the bottle. The sticky tape was applied on the back of the Cu substrate which was then placed on the inside of the cover of the bottle containing *Allium sativum*. The bottle was then tightly sealed with the cover. The distance between the chopped *Allium sativum* and Cu-substrate in the bottle was kept being 5 ± 1 cm and left at room temperature for 6–96 h. The obtained black Cu_7S_4 was dried at 60 °C for 2 h in the oven.

2.3 Materials characterization

The field emission scanning electron microscopy (SEM, Zeiss Supra 40) equipped with an energy dispersive X-ray (EDX) analyzer was conducted to characterize the surface morphology and elemental composition of the biosulfurized samples. Transmission electron microscopy (TEM, Tecnai G2-F20) was carried out to record both TEM and High-resolution TEM images of the obtained samples, and selected area electron diffraction (SAED) was applied to identify the lattice structure and structural nature of the samples. X-ray diffraction (XRD, CuKα radiation (λ = 1.5405 Å, nickel filter)) and X-ray photoelectron spectroscopy (XPS, Kratos, Axis Ultra-DLD) were employed to characterize the phase structure and chemical states of the obtained samples, respectively. The specific surface area and porosity of the sample were measured at 60 °C on a micromeritics ASAP 2020 using nitrogen (N_2) adsorption/desorption isotherms and Brunauer–Emmett–Teller (BET) method.

2.4 Electrochemical biosensing studies

The electrochemical behaviour of biosulfurized Cu_7S_4 on Cu substrates as electrodes in the absence and presence of glucose was evaluated using cyclic voltammetry (CV) and

chronoamperometry (CA) measurements. All electrochemical measurements were performed using an electrochemical workstation in an alkaline electrolyte (0.1 M NaOH with pH value of 13) aqueous solution using a three-electrode electrochemical cell composed of Cu_7S_4 on Cu-substrate as a working electrode (WE), a platinum (Pt) wire as an auxiliary/counter electrode (CE), and Ag/AgCl/(saturated KCl) as a reference electrode (RE). Cyclic voltammetry (CV) measurements were carried out in 0.1 M NaOH electrolyte under ambient conditions and recorded by varying the working electrode potential from −1.0 to 1.0 eV and scan rates of 20–280 mV s^{-1}. The chronoamperometric (CA) studies were performed by successive addition of known amounts of glucose concentrations (0.5, 1, 5, 10, 25, 50, 75 and 100 μM) into 0.1 M NaOH at applied potential of +0.5 eV.

3 Result and discussion

3.1 Surface morphology

The surface morphology and microstructures of biosulfurized Cu_7S_4 thin films were characterized by field emission scanning electron microscopy (SEM), transmission electron microscopy (TEM) and high-resolution transmission electron microscopy (HRTEM). Fig. 1a–c shows the morphologies and microstructures of Cu_7S_4 thin films at 96 h reaction time. Fig. 1a reveals the biosulfurized SEM image of Cu_7S_4 and exhibits vertically grown one dimensional (1D) hierarchical hollow nanotubes with long depth. The growth and morphology evolution process of Cu_7S_4 hollow particles was obtained at different reaction intervals/stages (or from 6–96 h) as shown in Fig. S1 (ESI materials).† At 6 h reaction time, the surface of Cu substrate is covered by small nanosphere like particles. When the reaction time was prolonged to 12, 24 and then to 48 h the Cu_7S_4 nanoparticles are growing vertically and become bigger and longer. Further extending the reaction stage to 72 h, the vertically grown particles are created a hollow at the top. Finally, well-defined 1D hierarchal Cu_7S_4 hollow nanotubes with a long depth are obtained after prolonged to 96 h. The average void/hollow diameter of Cu_7S_4 hollow nanotubes is ≈210 nm with a shell thickness of 52 nm, and average height of the nanotubes is ≈2.09 μm. Moreover, secondary dense nano-leaves like small particles are grown and surrounded the hollow nanotubes from external at the bottom. According to the results, the growth, morphological evolution, and formation mechanism of 1D hierarchical Cu_7S_4 hollow nanotubes could be attributed to the Ostwald ripening mechanism for the fabrication of hollow nanostructures. This Ostwald ripening process involves the growth and recrystallization of large particles with hollow interiors by sacrificing small aggregates.[37–40]

Further detailed structural characterizations of Cu_7S_4 were performed using TEM and HRTEM. Fig. 1b and c depicts the TEM images and scattered area electron diffraction (SAED) patterns of nanotubules Cu_7S_4 hollow nanotubules. From the TEM image in Fig. 1b, the dark edges and pale centers are observed, which provides convincing evidence of the Cu_7S_4 nanotubes have a hollow interior and cavities within the entire shell walls.[41,42] The HRTEM image of Cu_7S_4 (inset of Fig. 1b) reveals a series reflection fringe with a fringe spacing is 0.21 nm, attributed to the (0160) crystal plane of orthogonal Cu_7S_4, which is in good agreement with a literature[43] The crystallographic features of Cu_7S_4 were further recorded using SAED, and diffraction rings appear in the SAED patterns, as shown Fig. 1c. The uniform spots on rings confirm the perfect growth of the polycrystalline nature of Cu_7S_4.[44,45]

3.2 Structural and compositional analysis of Cu_7S_4 hollow nanotubes

The crystal phase and structure of the obtained sample were examined using X-ray diffraction (XRD) technique. Fig. 2a shows the XRD patterns of Cu_7S_4 hollow nanotubes exposed to 96 h to the organosulfur compounds of *Allium sativum* and several well-defined diffraction peaks at 2θ values of 24.16, 26.64, 29.22, 31.18, 33.76, 35.97, 37.18, 46.10, 48.44, and 53.98° are identified corresponding to (3,7,2), (16,0,0), (8,0,4), (18,2,1), (20,0,1), (20,4,0), (1,5,5), (0,8,6), (8,8,6), and (2,6,6) crystal planes. The diffraction peaks coincide with the peaks of orthorhombic anilite Cu_7S_4 crystal phase (JCPDS no. 23-0958),[46] and the strong diffraction peaks confirmed that the products are well-crystallized nanoparticles. The (0,8,6) peak at 2θ value of 46.10° is particularly intense, which confirms the preferential growth orientation of nanostructures with hollow-like surfaces[33] (confirmed by SEM image).

Fig. 2b shows the dispersive X-rays Spectroscopy (EDS) spectra of Cu_7S_4 hollow nanotubes and clearly reveals the presence of Cu and S elements, indicating the formation of

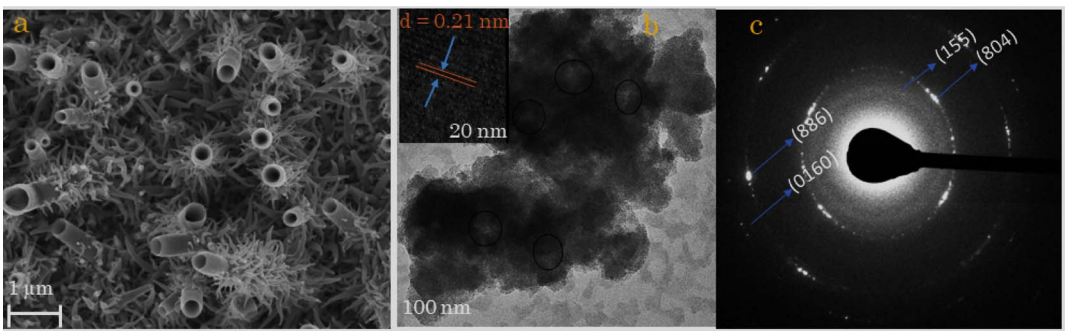

Fig. 1 (a) SEM image, (b) TEM image (inserted HRTEM), and (c) SAED of Cu_7S_4 at 96 h.

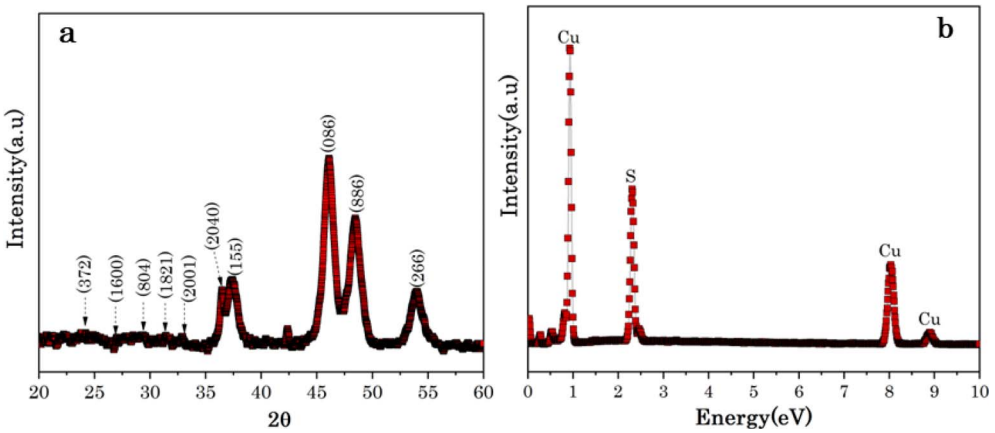

Fig. 2 (a) XRD patterns and (b) EDX spectra of Cu_7S_4 hollow nanotubes at 96 h.

Cu_7S_4. The Cu-substrates were exposed to organosulfur compounds of *Allium sativum* for different reaction stages from 6 to 96 h, as shown in Fig. S2 (ESI materials).† From the EDS spectra, the sulfur (S) peak located at 2.23 keV is almost non-existant for the lowest reaction stage of 6 h, while it becomes an intense peak after 12 h and increases with exposure time, even though it is dominated by the corresponding Cu peaks located at 0.91, 8.1, and 8.9 keV. Moreover, the EDS deduced relative ratio of Cu/S decrease, which confirms the S content increase with exposure time to the volatile organosulfur compounds of *Allium sativum*, as summarized in Table 1. Generally, the EDS analysis confirmed that the presence of continuous bio-sulfurization of Cu substrate surfaces and sulfurization saturates at Cu/S ~1, Table 1.

The surface chemical states and further elemental compositions of biosulfurized Cu_7S_4 hollow nanotubes were analysed *via* X-ray photoelectron spectroscopy (XPS). The Wider scan XPS survey of Cu_7S_4 confirms the presence of copper (Cu), sulfur (S), oxygen (O), and carbon (C) elements in Cu_7S_4, as displayed in Fig. 3a. Among them, O and C elements might derive from impurities and oxides on the Cu_7S_4 hollow nanotubules surfaces. The higher resolution XPS of Cu 2p core levels is shown in Fig. 3b, where two binding energy peaks are emerged at 953.4 and 932.2 eV, respectively are attributed to Cu $2p_{1/2}$ and Cu $2p_{3/2}$, which confirms the existence of Cu(I) in Cu_7S_4. From Fig. 3c, the high resolution XPS spectrum for S 2p at 163.5 and 162.2 eV binding energies which are associated to S $2p_{1/2}$ and S $2p_{3/2}$, respectively. In brief, the two XPS spectra of Cu 2p and S 2p corresponding to sulfides Cu_7S_4 proving the presence of Cu_7S_4 hollow nanotubes. Notably, the binding energies of S $2p_{3/2}$ and S $2p_{1/2}$ of Cu_7S_4 hollow nanotubes exhibits a slight shift to lower binding energies confirming that the higher electron configuration, resulting improved electronic conductivity of the Cu_7S_4 hollow nanotubes, which is highly favorable for accessing large amounts of analytes during electrochemical reactions.[33]

The specific surface area and pore size of Cu_7S_4 hollow nanotubes were analyzed from nitrogen (N_2) adsorption/desorption isotherms using the Brunauer–Emmett–Teller (BET) method as shown in Fig. 3d and exhibits a type III IUPAC classification, which confirms the mesoporous structure (2–50 nm) of the sample.[47] While the lower adsorption curve of the isotherm was used to measure the specific surface area, the desorption of isotherm was for pore size analysis. Based on the N_2 sorption results, the calculated BET surface area of Cu_7S_4 is 2.07 $m^2\ g^{-1}$, and the total pore volume is found to be 2.12 × 10^{-2} $cm^3\ g^{-1}$. The pore size distribution (inset in Fig. 3d) of the sample is centered at 27.90 nm, further confirming the existence of mesopores structure for Cu_7S_4 hollow nanotubes. The specific surface area and pore size have significant effects on the adsorption properties and catalytic active sites of biosensor nanomaterials.[48]

Table 1 EDS deduced relative ratio of Cu/S with the exposure time to volatile organosulfur compounds of *Allium sativum*

Reaction stages (hours)	Cu intensity	S intensity	Relative ratio Cu/S
6	29 478.2	6272.7	4.70
12	62 095.0	32 431	1.91
24	90 938.1	66 131.3	1.37
48	113 234.8	96 921.4	1.16
72	131 741.5	120 630.2	1.09
96	149 312.2	139 419.6	1.06

3.3 Electrochemical non-enzymatic glucose detection

The pH impact on electrochemical glucose detection by Cu_7S_4 hollow nanotubes electrode was explored, and Fig. 4 shows the CV curves of Cu_7S_4 hollow nanotubes at pH values of 2.5, 5, 7.5, and 10 with 60 μM glucose in 0.1 M NaOH solution a scan rate of 50 mV s^{-1}. The area of the CV current increased from pH 2.5 to 7.5; however, the redox reactions are not clearly visible, and the CV curve shape is distorted compared to the higher pH values. From the CV, the glucose oxidation reactions at pH 10 and 13 are barely detectable and the glucose oxidation peaks current increased with increasing the pH value from 10 to 13. The pH value of 13 for the 0.1 M NaOH electrolyte was determined to be the optimal experimental parameter Cu_7S_4 hollow nanotubes electrode for the electrochemical non-enzymatic glucose detection that will be used next.

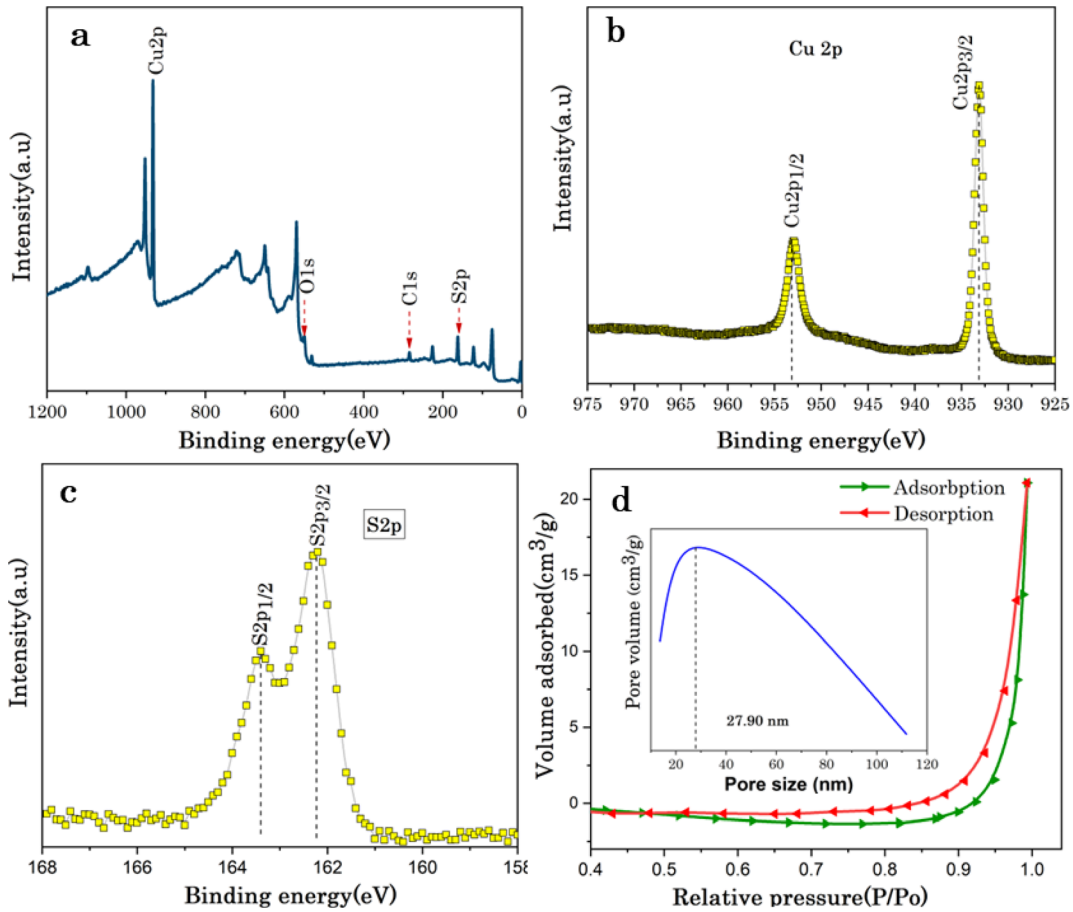

Fig. 3 (a) Wide scan XPS survey of Cu_7S_4 hallow nanotubes; XPS spectrum (b) Cu 2p, (c) S 2p; (d) nitrogen (N_2) adsorption/desorption isotherms (insert pore size distribution curve of Cu_7S_4 hallow nanotubes).

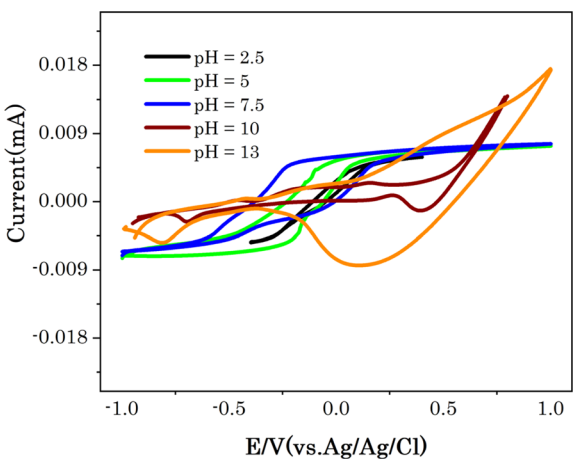

Fig. 4 CV curves of Cu_7S_4 at different pH values in 0.1 M NaOH solution with 60 μM glucose at scan rate of 50 mV s^{-1}.

The electrochemical response of Cu_7S_4 hollow nanotubes electrode in the absence and presence of glucose was investigated using cyclic voltammetry (CV) in 0.1 M NaOH solution as electrolyte to explore the electrocatalytic activities. All CVs were performed in the potential window between −1.0 to 1.0 eV, which covers the glucose electro-oxidation range in alkaline electrolytes. Fig. 5 shows CVs of Cu_7S_4 hollow nanotubes without and with 60 μM glucose in 0.1 M NaOH solution at scan rate of 20 mV s^{-1}. In the presence of glucose, Cu_7S_4 hollow nanotubes electrode displayed a higher catalytic current density compared without glucose attributed to the high electrocatalytic surface area and catalytic ability of Cu_7S_4 hollow nanotubes. The enhanced electrocatalytic current response of Cu_7S_4 hollow nanotubes towards the oxidation of glucose occurs due to its hollow nanostructures, which offer a higher active surface area, good electronic conductivity, and the presence of a void-like open structure configuration (as confirmed from SEM image) in Cu_7S_4 hollow nanotublets allows access to large amount of glucose molecules to the inner and outer surfaces for efficient glucose oxidation.[29,33]

The effect of scan rate was investigated to determine the reaction kinetics of Cu_7S_4 hollow nanotubes in 0.1 M NaOH electrolyte containing 60 μM of glucose. Fig. 6a displays the CV responses of glucose oxidation on Cu_7S_4 hollow nanotubes surface for different scan rates ranging from 20 to 280 mV s^{-1}. The oxidation (anodic) and reduction (cathodic) peak current of glucose at Cu_7S_4 increases with scan rates. Moreover, the reduction peak current is fully associated with the reduction of Cu(II) to Cu(I) and has shifted towards the more negative region

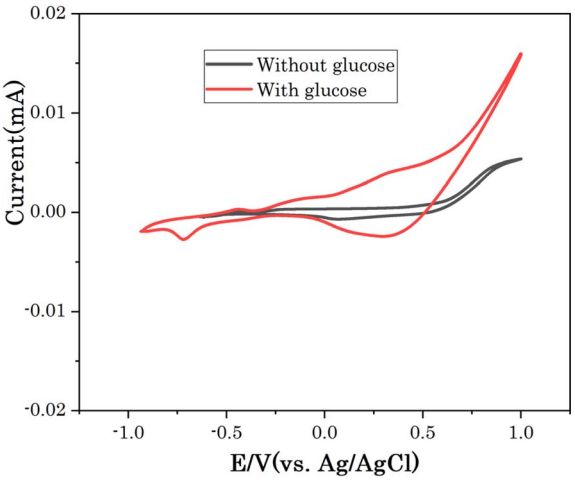

Fig. 5 CV of Cu_7S_4 electrode in 0.1 M NaOH solution without and with 60 μM glucose at scan rate of 20 mV s^{-1}.

with scan rates, suggesting a quasi-reversible electron transfer reaction of glucose.[49] Both anodic peak current (I_{pa}) and cathodic peak current (I_{pc}) are plotted against the scan rates as shown in Fig. 6b and are directly proportional to the square root of scan rates. This confirms that the redox peak current on hollow Cu_7S_4 nanotube electrode are diffusion controlled electrochemical processes.[49,50] The regression equations between the peak current and square root of the scan rates can be expressed using eqn (1) and (2) given below.[51,52]

$$I_{pa}(\text{mA}) = (0.00209 \pm 0.00037) \times V^{\frac{1}{2}}(\text{mV s}^{-1}) - (2.12 \pm 0.0307), \quad R^2 = 0.983 \tag{1}$$

$$I_{pc}(\text{mA}) = (-0.00116 \pm 0.00029) \times V^{\frac{1}{2}}(\text{mV s}^{-1}) + (2.24 \pm 0.0036), \quad R^2 = 0.996 \tag{2}$$

The non-enzymatic electrochemical sensing was investigated on Cu_7S_4 electrodes surface using chronoamperometry (CA) in 0.1 M NaOH solution with successive additions of known amounts of glucose concentrations at +0.5 eV. Fig. 7A and B shows the chronoamperometric responses of biosulfurized of Cu_7S_4 hollow nanotubes under successive injection of different glucose contents of 0.5, 1, 5, 10, 25, 50, 75 and 100 μM and the corresponding calibration curves. The electrocatalytic oxidation current of glucose exhibits a wide linear response and increases with increasing concentration of glucose in the given order from 0.5 μM to 100 μM, as shown in Fig. 7A.

The corresponding calibration plot was obtained by plotting the amperometric current *versus* glucose concentrations for Cu_7S_4 hollow nanotubes and notably, an observable linear correlation emerged between the concentrations of glucose and the ensuing current response, as illustrated in Fig. 7B. This correlation is effectively encapsulated by a linear regression model: current (μA) = 0.058 + 0.023C (μmol L^{-1}), indicating an acceptable coefficient of determination (R^2) value of 0.99. Crucially, through eqn (3), the limit of detection (LOD) for glucose detection is robustly estimated to be 0.127 μmol L^{-1}.

$$\text{LOD} = \frac{3s}{m} \tag{3}$$

where "*s*" represents standard error, and "*m*" represents the slope of the current in relation to the concentrations. The biosulfurized Cu_7S_4 hollow nanotube electrode on Cu-substrate has a high sensitivity of 1058.33 μA mM^{-1} cm^{-2}, extremely higher when compared with the sensitivity of 361.58 μA mM^{-1} cm^{-2} reported for Cu/CuS.[53] In addition to the inherent properties, the interior cavities and similar particle size (see SEM image) in Cu_7S_4 hollow nanotubes could reduce the diffusion distance or energy barriers and provide large surface area as well as more active sites to facilitates accessing large amount of glucose for efficient oxidation.[33,46,54]

The analytical performances of the developed Cu_7S_4 hollow nanotube electrode towards non-enzymatic glucose sensors are compared with other Cu_xS based non-enzymatic glucose

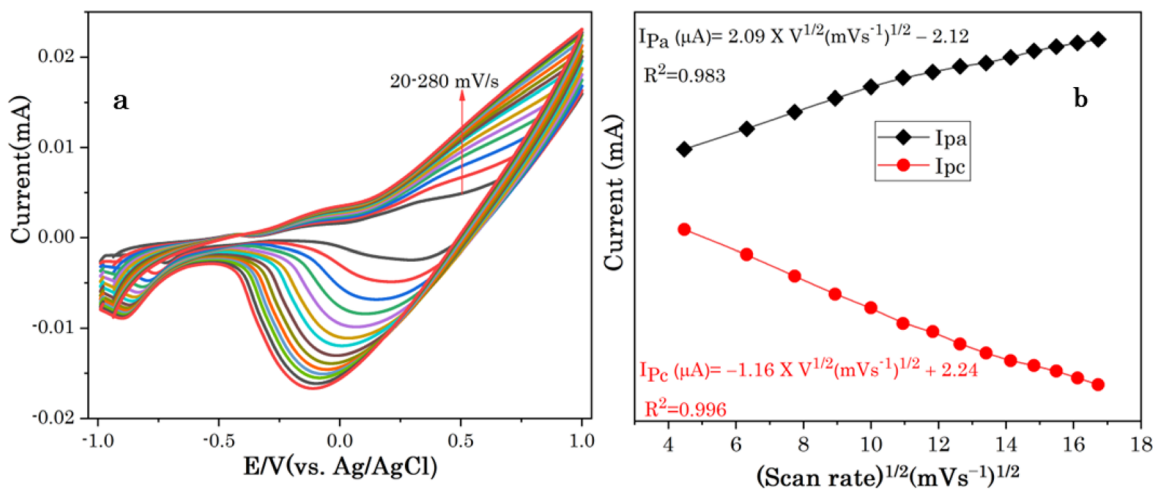

Fig. 6 (a) CVs of Cu_7S_4 at different scan rates from 20 to 280 mV s^{-1} in a 0.1 M NaOH solution in the presence of 60 μM glucose, (b) the corresponding plots of anodic and cathodic peak currents.

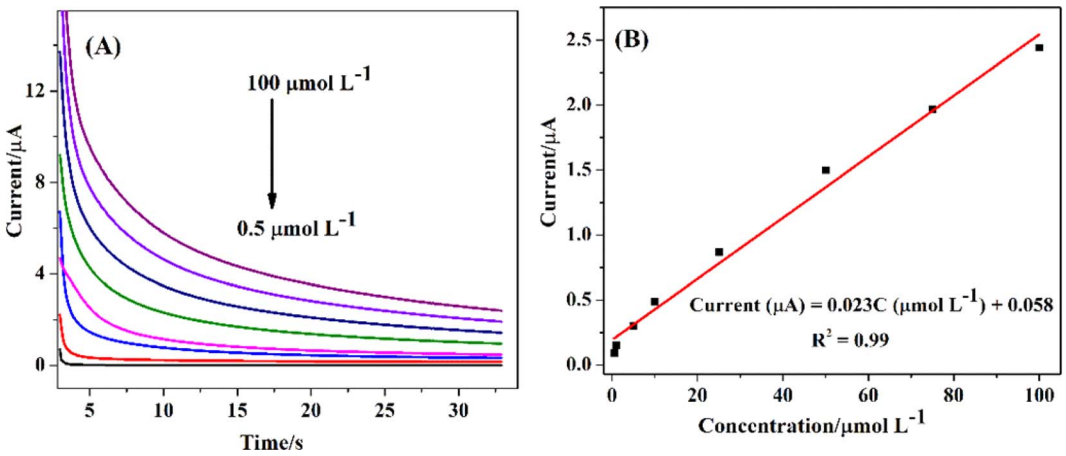

Fig. 7 (A) Chronoamperometry response to various glucose concentrations (0.5 to 100 μmol L^{-1}) and (B) the corresponding calibration curves for Cu_7S_4 hollow nanotubes.

sensors previously reported using analytical parameters of linear range, limit of detection (LOD) and sensitivity as shown in Table 2. In conclusion, it is important to mention that surface morphology, high specific surface area, nanostructure porosity, and composition have crucial role in the electrocatalytic performance of nanomaterials.[33,60,61]

3.4 Specificity and reproducibility of Cu_7S_4 hollow nanotubes

The avoidance of interfering species is still challenging for non-enzymatic glucose determination, because some organic molecules with a similar structure such as uric acid (UA), ascorbic acid (AA), oxalic acid (OA), fructose (Fru) *etc.*, are co-existing in the biological fluids and simultaneously catalysed with glucose and generate interfering electrochemical signals.[29] The selectivity of Cu_7S_4 hollow nanotubes was evaluated by measuring electrochemical signals in the presence of other sugars and other oxidizable interfering species. Considering that the concentration of glucose in human blood is more than 30 times of the physiological interfering compounds, thus, normal physiological concentrations of 50 μM glucose and 10 M of interferences of uric acid (UA), ascorbic acid (AA), oxalic acid (OA), Fructose (Fru), Galactose (Gla), lactose (LA), H_2O_2, Na^+, and NO_3^- were orderly added into 0.1 M NaOH solution at 0.5 V as shown in Fig. 8a. The sharp response is observed for the addition of 50 μM glucose and no significant current increase is detected upon the addition of UA, AA, OA, H_2O_2, Na^+, and NO_3^-, suggesting that these species do not interfere with glucose determination. Similarly, no obvious responses upon the addition of carbohydrate derivatives (*i.e.* Fru, Gla and La) is observed as shown Fig. 8a. The increase in current density observed again after the second injection of Glu reveals that Cu_7S_4 hollow nanotubes are still sensitive to Glu, and their activity is not compromised by the interferents. Thus, this study demonstrated that the hierarchical Cu_7S_4 hollow nanotubes reveal a high specificity or selectivity in the presence of co-interfering species toward glucose detection.

The stability and reproducibility of the Cu_7S_4 hollow nanotubes sensor were also evaluated. Fig. 7B depicts the chronoamperometry stability of Cu_7S_4 hollow nanotubes which reveals a sharp response for the addition of 50 μM glucose in 0.1 M NaOH. Afterwards, a steady state current was achieved for 1200 seconds(s) confirming that the Cu_7S_4 hollow nanotubes glucose detecting electrode has good operational stability. Moreover, to ascertain the reproducibility of the Cu_7S_4 hollow nanotubes, the chronoamperometric response to the repeated addition of 50 μM D-glucose was tested by 6 repeated measurements, as shown in Fig. 9 and the proposed biosensor

Table 2 Comparison Cu_7S_4 hollow nanotubes electrode with previously reported Cu_xS-based electrodes for non-enzymatic glucose defection from literature

Electrode	Linear range (μmol L^{-1})	LOD (μmol L^{-1})	Sensitivity (μA mM^{-1} cm^{-2})	Ref.
Cu/Cu_7S_4 hollow nanotubes	0.5–100	0.127	1058.33	This work
Cu_2S nanoparticles	10–3000	1.3	61.67	55
Au-Cu_xS/3DCF	1.98–976.56	7.62	59	56
Cu@CuS	2–8100	0.10	361.58	53
Cu_2S nanocrystal-DWCNT/GCE	0.005–1	1	280	57
S-rGO/CuS	0.0001–3880	0.032	429.4	51
CuS nanosphere-like	1.0–1200	0.015	117.3	58
Cu_2S/MWCNT	0.0010–1000	1.0	0.075	59

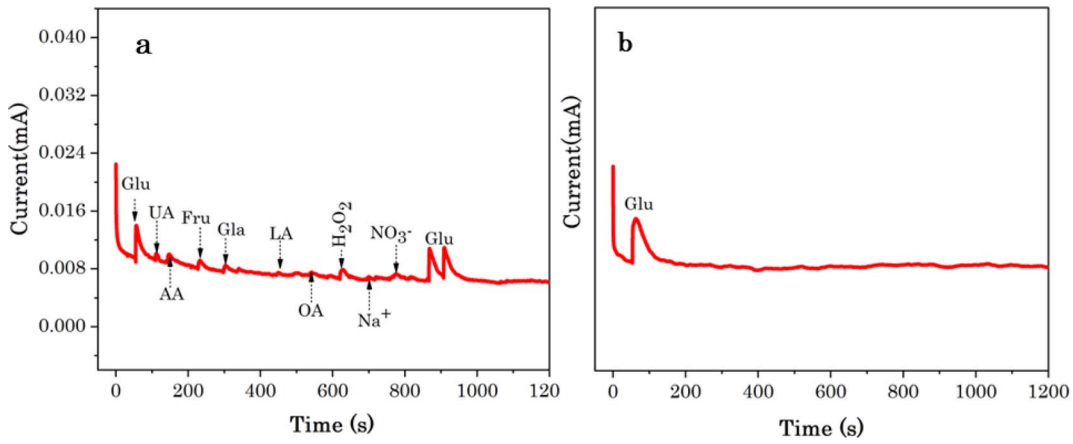

Fig. 8 (a) Chronoamperometric current response of Cu_7S_4 hollow nanotubes to 50 μM glucose and 10 μM interferents 0.1 M NaOH (b) the chronoamperometric stability test conducted at Cu_7S_4 hollow nanotubes electrode with the addition of 50 μM glucose in 0.1 M NaOH.

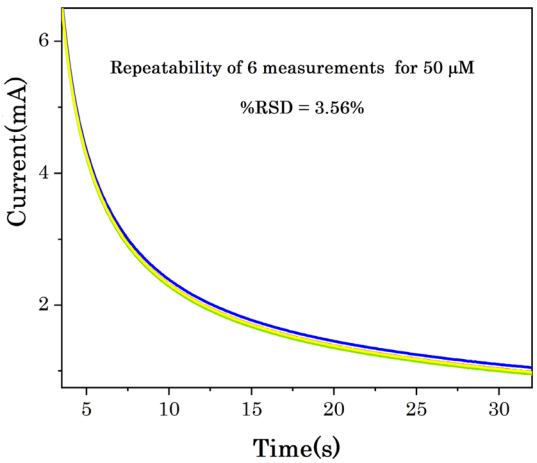

Fig. 9 Chronoamperometric response of Cu_7S_4 hollow nanotubes to the repeated addition of 50 μM glucose in 0.1 M NaOH.

electrode exhibits good repeatability with a relative standard deviation (RSD) of 3.56%. The observed results confirmed that the Cu_7S_4 hollow nanotubes electrode has good stability and reproducibility for glucose detection.

4 Conclusion

In conclusion, low-dimensional nanomaterials with distinguishable interior hollows and shells have advantages of offering high surface areas, increased reactivities, and unique physicochemical properties for efficient biosensing applications. This work presents a novel approach for the bio-sulfurization of 1D hierarchical hollow Cu_7S_4 nanotubelets as electrode materials through the application of volatile organosulfur compounds. Characterization techniques confirmed the successful fabrication of hierarchical hollow nanostructures, revealing their distinct morphology and composition. The bio-sulfurized Cu_7S_4 hollow nanotube electrochemical sensor ascribed efficient performance as non-enzymatic electrochemical glucose detection. Interestingly, the detection of glucose was conducted over a dynamic range of concentrations ranges from 0.5 to 100 μmol L^{-1}, with a limit of detection (LOD) of 0.127 μmol L^{-1}. The Cu_7S_4 hollow nanotubes exhibited an excellent electro-catalytic activity towards glucose oxidation with a high sensitivity of 1058.33 μA mM^{-1} cm^{-2}. Furthermore, it demonstrates also a high selectivity in the potentially co-interfering ions toward glucose determination. The inherent properties of Cu_7S_4 hollow nanotube surfaces, coupled with the bio-sulfurization process mediated by volatile organosulfur compounds of *Allium sativum* L contribute to enhanced sensitivity and selectivity towards glucose detection. This innovative green bio-approach holds significant promise for the development of advanced glucose sensing technologies with potential applications in biological samples.

Data availability

The data supporting this article are available within the paper and the ESI.†

Conflicts of interest

There are no conflicts to declare.

Acknowledgements

This work was supported by the Department of Science and Innovation (DSI) and National Research Foundation (NRF), South Africa through DSTI/NRF South African Research Chairs Initiative for Professor of Medicinal Chemistry and Nanotechnology (UID 62620), DSI/Mintek Nannotechnology Innovation Centre, and Rhodes University (for materials and postdoctoral research fund for G. G. W.), South Africa. The authors give credit to ithemba labs MRD, Cape town, South Africa for the characterizations.

References

1 Y. Huo, R. Li, S. Xiu, Y. Wang, L. Zhang, A. Jin and B. Quan, *Diamond Relat. Mater.*, 2023, **140**, 110455–110463.
2 B. Tao, H. Zheng, J. Li, F. Miao and P. Zhang, *Mater. Sci. Eng., B*, 2017, **298**, 116895.
3 D. Das, A. Das, M. Reghunath and K. K. Nanda, *Green Chem.*, 2017, **19**, 1327–1335.
4 S. Kumar, M. B. Gawande, I. Medřík, M. Petr, O. Tomanec, V. Kupka, R. S. Varma and R. Zbořil, *Green Chem.*, 2020, **22**, 5619–5627.
5 S. Yu, R. D. Webster, Y. Zhou and X. Yan, *Catal. Sci. Technol.*, 2017, **7**, 2050–2056.
6 P. Bhavani, D. P. Kumar, H. S. Shim, P. Rangappa, M. Gopannagari, D. A. Reddy, J. K. Song and T. K. Kim, *Catal. Sci. Technol.*, 2020, **10**, 3542–3551.
7 W. Lu, R. Zhang, X. Zhang, Y. Shi, Y. Wang and H. Shi, *Analyst*, 2023, **148**, 5469–5475.
8 A. D. Ambaye, T. G. Kebede, B. Ntsendwana and E. N. Nxumalo, *Synth. Met.*, 2023, **299**, 117452.
9 N. Njoko, M. Louzada, J. Britton, S. Khene, T. Nyokong and P. Mashazi, *Colloids Surf., B*, 2020, **190**, 110981.
10 M. Wei, Y. Qiao, H. Zhao, J. Liang, T. Li, Y. Luo, S. Lu, X. Shi, W. Lu and X. Sun, *Chem. Commun.*, 2020, **56**, 14553–14569.
11 P. Wu, J. Fan, Y. Tai, X. He, D. Zheng, Y. Yao, S. Sun, B. Ying, Y. Luo, W. Hu, X. Sun and Y. Li, *Food Chem.*, 2024, **447**, 139018.
12 D.-W. Hwang, S. Lee, M. Seo and T. D. Chung, *Anal. Chim. Acta*, 2018, **1033**, 1–34.
13 S. Wang, L. Zhao, R. Xu, Y. Ma and L. Ma, *Electroanal. Chem.*, 2019, **853**, 113527.
14 J. Lv, C. Kong, Y. Xu, Z. Yang, X. Zhang, S. Yang, G. Meng, J. Bi, J. Li and S. Yang, *Sens. Actuators, B*, 2017, **248**, 630–638.
15 L. Goodnight, D. Butler, T. Xia and A. Ebrahimi, *Biosensors*, 2021, **11**, 409.
16 H. Siampour, S. Abbasian, A. Moshaii and A. R. Amirsoleimani, *Sci. Rep.*, 2022, **12**, 18945.
17 C. Wei, X. Zou, Q. Liu, S. Li, C. Kang and W. Xiang, *Electrochim. Acta*, 2020, **334**, 135630.
18 O. Adeniyi, N. Nwahara, D. Mwanza, T. Nyokong and P. Mashazi, *Sens. Actuators, B*, 2021, **348**, 130723.
19 M. Bisht, S. K. Thayallath, P. Bharadwaj, G. Franklin and D. Mondal, *Green Chem.*, 2023, **25**, 4591–4624.
20 F. Zhou, C. You, Q. Wang, Y. Chen, Z. Wang, Z. Zeng, X. Sun, K. Huang and X. Xiong, *Electroanal. Chem.*, 2020, **876**, 114477.
21 G. G. Welegergs, G. G. Welegergs, H. G. Gebretnisae, M. G. Tsegay, Z. Y. Nuru, S. Dube and M. Maaza, *Infrared Phys. Technol.*, 2011, **113**, 103619.
22 G. G. Welegergs, Z. M. Mehabaw, H. G. Gebretinsae, M. G. Tsegay, L. Kotsedi, Z. Khumalo, N. Matinisie, Z. T. Aytuna, S. Mathur, Z. Y. Nuru, S. Dube and M. Maaza, *Infrared Phys. Technol.*, 2023, 104820.
23 X. Li, J. Cao, L. Yang, M. Wei, X. Liu, Q. Liu, Y. Hong, Y. Zhou and J. Yang, *Dalton Trans.*, 2019, **7**, 2442–2454.
24 M. P. Ravele, O. A. Oyewo, S. Ramaila, L. Mavuru and D. C. Onwudiwe, *Catalysts*, 2021, **11**, 1238.
25 B. Janani, R. Balakrishnaraja, A. M. Elgorban, A. H. Bahkali, R. S. Varma, A. Syed and S. S. Khan, *J. Environ. Manage.*, 2023, **326**, 116615–116626.
26 S. Farhadi and F. Siadatnasab, *Mater. Res. Bull.*, 2016, **83**, 345–353.
27 S. Saeed, N. Rashid, R. Hussain, M. A. Malik, P. O'Brien and W.-T. Wong, *J. Chem.*, 2023, **37**, 3214–3221.
28 G. G. Welegergs, N. Numan, S. Dube, Z. Nuru, N. Botha, K. Cloete, S. Azizi, I. Madiba, M. Akbari, R. Morad, M. G. Tsegay, H. G. Gebretinsae, C. Mtshali, Z. Khumalo, F. Ezema, A. Krief, A. Gibaud, M. Henini, M. P. Seopela, M. Chaker and M. Maaza, *Nanoscale Horiz.*, 2023, **2**, 1–27.
29 X. Yan, Y. Gu, C. Li, B. Zheng, Y. Li, T. Zhang, Z. Zhang and M. Yang, *Anal. Methods*, 2018, **10**, 381–388.
30 H. T. Zhang, G. Wu and X. H. Chen, *Mater. Chem. Phys.*, 2006, **98**, 298–303.
31 L. Qian, J. Mao, X. Tian, H. Yuan and D. Xiao, *Sens. Actuators, B*, 2013, **176**, 952–959.
32 S. Radhakrishnan, H.-Y. Kim and B.-S. Kim, *Sens. Actuators, B*, 2016, **233**, 93–99.
33 M. Cao, H. Wang, P. Kannan, S. Ji, X. Wang, Q. Zhao, V. Linkov and R. Wang, *Appl. Surf. Sci.*, 2019, **492**, 407–416.
34 X. Li, N. Li, Y. Gao and L. Ge, *Chin. J. Catal.*, 2022, **43**, 679–707.
35 L. Cong, H. Xie and J. Li, *Adv. Energy Mater.*, 2017, **7**, 1601906.
36 Z. Xu, Z. Qiu, Q. Liu, Y. Huang, D. Li, X. Shen, K. Fan, J. Xi, Y. Gu, Y. Tang, J. Jiang, J. Xu, J. He, X. Gao, Y. Liu, H. Koo, X. Yan and L. Gao, *Nat. Commun.*, 2018, **9**, 3713.
37 B. Zhao, G. Shao, B. Fan, W. Zhao, Y. Xie and R. Zhang, *J. Mater. Chem. A*, 2015, **3**, 10345–10352.
38 M. Cao, H. Lian and C. Hu, *Nanoscale*, 2010, **2**, 2619–2623.
39 W.-S. Wang, L. Zhen, C.-Y. Xu, J.-Z. Chen and W.-Z. Shao, *ACS Appl. Mater. Interfaces*, 2019, **1**, 780–788.
40 J.-X. Cui, W.-S. Wang, L. Zhen, W.-Z. Shao and Z.-L. Chen, *CrystEngComm*, 2012, **14**(20), 7025–7030.
41 G. Cheng and A. R. Hight Walker, *Anal. Bioanal. Chem.*, 2010, **396**, 1057–1069.
42 M. Basu, A. K. Sinha, M. Pradhan, S. Sarkar and T. Pal, *J. Phys. Chem. C*, 2011, **115**, 12275–12282.
43 Y. Jiang, S. Zhang, Q. Ji, J. Zhang, Z. Zhang and Z. Wang, *J. Mater. Chem. A*, 2014, **2**, 4574–4579.
44 W. Xu, S. Zhu, Y. Liang, Z. Li, Z. Cui, X. Yang and A. Inoue, *Sci. Rep.*, 2015, 18125.
45 J. Liu and D. Xue, *J. Mater. Chem.*, 2011, **21**, 223–228.
46 J. Hu, J. Yang, S. Yi, X. Zhou and S. Chen, *J. Energy Storage*, 2024, **77**, 109901.
47 C. Nethravathi, R. Ragesh Nath, J. T. Rajamathi and M. Rajamathi, *ACS Omega*, 2019, **4**, 4825–4831.
48 Z. Huang, L. Wang, H. Wu, H. Hu, H. Lin, L. Qin and Q. Li, *J. Alloys Compd.*, 2022, **896**, 163045.
49 L. Jayasingha, C. Jayathilak, R. Kumar, K. Ohar, M. Kaumal, S. Gunewardene, D. Dissanayake and S. Jayanetti, *Electrochim. Acta*, 2020, **329**, 135177.

50 W. Lu, Y. Sun, H. Dai, P. Ni, S. Jiang, Y. Wang, Z. Li and Z. Li, *Sens. Actuators, B*, 2016, **231**, 860–866.
51 N. Karikalan, R. Karthik, S.-M. Chen, C. Karuppiah and A. Elangovan, *Sci. Rep.*, 2017, **7**, 2494.
52 A. D. Ambaye, K. K. Kefeni, T. G. Kebede, B. Ntsendwana, S. B. Mishra and E. N. Nxumalo, *J. Electroanal. Chem.*, 2022, **919**, 116542.
53 X. Zhang, L. Wang, R. Ji, L. Yu and G. Wang, *Electrochem. Commun.*, 2012, **24**, 53–56.
54 Q. Chen, D. Chu, L. Yan, H. Lai, X. Q. Chu, D. Ge and X. Chen, *New J. Chem.*, 2021, **45**, 10031–10039.
55 S. K. Maji, A. K. Dutta, G. R. Bhadu, P. Paul, A. Mondal and B. Adhikary, *J. Mater. Chem. A*, 2013, **1**, 4127–4134.
56 L. N. T. Mai, S. Radhakrishnan and J. Mathiyarasu, *Electrochim. Acta*, 2017, **246**, 544–552.
57 Y. Myung, D. M. Jang, Y. J. Cho, H. S. Kim, J. Park, J.-U. Kim, Y. Choi and C. J. Lee, *J. Phys. Chem. C*, 2009, **113**, 1251–1259.
58 W. Wang, L. Zhang, S. Tong, X. Li and W. Song, *Biosens. Bioelectron.*, 2009, **25**, 708–714.
59 H. Lee, S. W. Yoon, E. J. Kim and J. Park, *Nano Lett.*, 2007, **7**, 778–784.
60 J. Ding, S. Ji, H. Wang, J. Key, D. J. Brett and R. Wang, *J. Power Sources*, 2018, **374**, 48–54.
61 J. Zhang, Y. Xu and B. Zhang, *Chem. Commun.*, 2014, **50**, 13451–13453.